Journal of Korean Society of
Coastal and Ocean Engineers
Vol. 12, No. 3, pp. 116~129, September 2000

Wave Deformation by Submerged Flexible Circular Disk
몰수된 원형 유연막에 의한 파랑변형

Il-Hyoung Cho* and Moo Hyun Kim**
조일형* · 김무현**

Abstract □ The interaction of incident monochromatic waves with a tensioned, flexible, circular membrane submerged horizontally below free surface is investigated in the frame of three-dimensional linear hydro-elastic theory. The velocity potential is split into two parts i.e. the diffraction potential representing the scattering of incident waves by a rigid circular disk and the radiation potential describing motion induced waves by elastic responses of flexible membrane. The fluid domain is divided into three regions, and the diffraction and radiation potentials in each region are expressed by the Fourier Bessel series. The displacement of circular membrane is expanded with a set of natural functions, which satisfy the membrane equation of motion and boundary conditions. The unknown coefficients in each region are determined by applying the continuity of pressure and normal velocity at the matching boundaries. The results show that various types of wave focusing are possible by controlling the size, submergence depth, and tension of membrane.

Keywords : hydro-elastic theory, eigenfunction expansion method, flexible circular disk, diffraction, radiation

要　旨 : 자유수면 아래 일정한 초기장력이 작용한 원형 박막이 수평으로 놓여있을 때 3차원 선형 유탄성 이론을 적용하여 파와 구조물의 상호작용문제를 고찰하였다. 속도포텐셜을 회절포텐셜과 방사포텐셜로 분리하여 각각의 경계치 문제를 푼다. 유체영역을 3개의 영역으로 나누어 각 영역에서 회절포텐셜과 방사포텐셜을 Bessel 함수의 전개식으로 표현하고 부족한 경계조건으로 생기는 미지수는 인접한 영역이 만나는 정합면에서 속도와 압력이 같다는 정합조건식을 적용하여 구해진다. 원형막의 크기와 잠긴 깊이 그리고 초기장력이 변함에 따라 원형 유연막 주위의 파의 형태가 달라짐을 볼 수 있었다. 즉, 적절히 설계된 몰수형 원형 유연막은 파 에너지를 집중시키는데 활용될 수 있다.

핵심용어 : 유탄성 이론, 고유함수 전개법, 원형 유연막, 회절, 방사

1. INTRODUCTION

Various wave barriers using flexible membrane have been proposed for the temporary protection of coastal regions and construction sites. The flexible membrane is easy to carry, inexpensive, reusable, and rapidly deployable and removable, and therefore, can be used for a variety of coastal/ocean applications, which require rapid and cost-effective solutions. The flexible membrane may also be used as a device for focusing or spreading wave energy. In this paper, the deformation of plane monochromatic incident waves by a submerged flexible circular disk is investigated.

The interaction of incident waves with a two-dimensional vertical membrane in tension has been investigated by Thomson *et al.* (1992), Kim and Kee (1996), and Kee and Kim (1997), and Williams (1996). They used a tensioned-string dynamic model to solve the motion of the tensioned membrane per unit length. The tensioned membrane can be considered as the limiting case of the ten-

*제주대학교 해양산업공학부 (Faculty of Marine Industrial Engineering, Cheju University, Ara 1, Cheju 690-756, Korea)
**텍사스 A&M대학교 토목공학과 (Department of Civil Engineering, Texas A & M University, College Station, Texas, 77843, USA)

sioned-beam plate as the bending stiffness approaches zero. The performance of the elastic-beam wave barrier clamped at the seafloor without tension was investigated by Lee and Chen (1990) and Williams *et al.* (1991). Cho and Kim (1998) recently studied the performance of a tensioned horizontal flexible membrane as a wave barrier and their experimental results reasonably followed their numerical predictions.

On the other hand, the diffraction of incident waves by a submerged rigid circular disk in the horizontal plane was investigated by Yu and Chwang (1993). By means of the separation of variables, the fluid domain was divided into three regions and the scattering potentials in each region were expressed by the product of unknown coefficients and the Bessel functions. The unknown coefficients were determined by applying the matching conditions at the common boundaries of neighboring regions. The resulting wave field around the disk was shown for various incident wave conditions and disk parameters. They also showed that wave focusing was apparent, in some cases, near the rear of the disk.

In this paper, the interaction of plane monochromatic waves with a tensioned, flexible, circular membrane suberged in the horizontal plane, is investigated in the context of linear hydro-elastic theory. The initial tension is assumed to be uniform in the radial direction and the edge of the membrane is assumed to be fixed in space. The vertical displacement of the circular membrane is represented by a series expansion using natural functions. The natural functions and membrane responses are obtained by solving the two-dimensional wave equation given in polar coordinate with specified boundary conditions. The diffraction and radiation potentials are solved by means of the eigen-function expansion method. The solutions are separately obtained in each sub-region and they are matched at the common vertical boundaries.

The primary concern in this study is the deformation of incident wave field by the presence of a tensioned, flexible, circular membrane submerged in the horizontal plane. Sec.2 describes mathematical formulation of diffraction and radiation problems and membrane dynamics. Various numerical examples are presented and the results discussed in Sec.3. Concluding remarks are given in Sec.4.

2. MATHEMATICAL FORMULATION

We consider a horizontally submerged flexible-membrane disk of radius a, as shown in Fig. 1. For analysis, a polar coordinate system (r, θ, y) is chosen with the origin on the undisturbed free surface and y-axis pointing vertically upwards. The depth of water is denoted by h and the submergence depth of membrane by d. The tension T is applied uniformly on the membrane in the radial direction. The water is assumed to be incompressible and inviscid, so that the fluid particle motion can be described by a velocity potential Φ. It is also assumed that wave and membrane motions are small to allow linear hydro-elastic theory for the present study.

Under the assumptions stated above, the velocity potential and the vertical displacement of membrane can be written as

$$\Phi(r,\theta,y,t)=\Re[\phi(r,\theta,y)e^{-i\omega t}]$$
$$\zeta(r,\theta,t)=\Re[\xi(r,\theta)e^{-i\omega t}] \quad (1)$$

where ω is the angular frequency of monochromatic incident waves and $\xi(r, \theta)$ is the complex displacement of membrane motions.

The complex displacement of membrane may be expanded as follows using a set of natural modes:

$$\zeta(r,\theta)=\sum_{p=0}^{\infty}\sum_{j=1}^{\infty}\varsigma_{pj}w_{pj}(r,\theta) \quad (2)$$

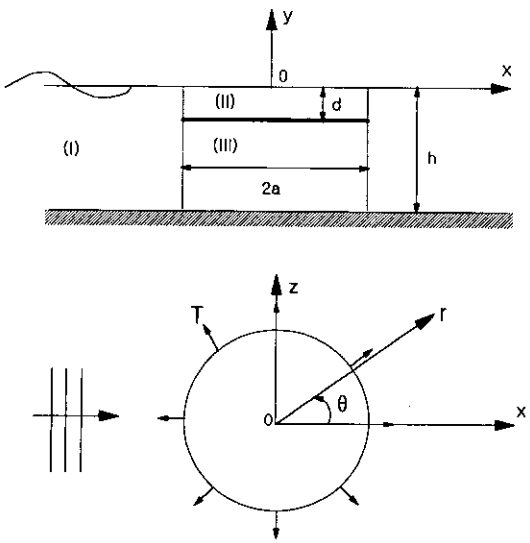

Fig. 1. Definition Sketch of Horizontal Disk Membrane.

where ς_{pj} is the unknown complex amplitude corresponding to the (p, j) th mode. The value of (p, j) denotes the number of natural modes in the (θ, r) direction, respectively. The natural functions and frequencies of the membrane can be easily obtained by the membrane equation of motion with the fixed-end conditions.

$$w_{pj}(r,\theta)=J_p(\Omega_{pj}r/a)\cos p\theta \tag{3}$$

where Ω_{pj} are the zeros of $J_p(\Omega_{pj})=0$, p=0, 1, 2, 3,... The values of these zeros are available in Abramowitz and Stegun (1972).

The natural functions $w_{pj}(r, \theta)$ in Eq. (3) satisfy the following orthogonal relation:

$$N_{qi}=\int_0^{2\pi}\int_0^a rw_{qi}(r,\theta)w_{pj}(r,\theta)\,drd\theta$$
$$=\begin{cases}\dfrac{a^2}{2}(1+\delta_{p0})\pi J_P^2(\Omega_{pi}), p=q \text{ and } i=j\\ 0 \quad \text{otherwise}\end{cases} \tag{4}$$
$$p,q=0,1,2\ldots$$

The symbol δ_{p0} is Kronecker delta function by δ_{00}=0, δ_{p0}=0, p=1,2,... Guided by the expansion of membrane motion, the velocity potential $\phi(r, \theta, y)$ can be written in the form:

$$\phi(r,\theta,y)=-\frac{igA}{\omega}\sum_{p=0}^{\infty}\left\{\phi_D^p(r,y)+\sum_{j=0}^{\infty}\varsigma_{pi}\phi_{Rj}^p(r,y)\right\}\cos p\theta$$

$$\phi_D^p(r,y)=\phi_I^p(r,y)+\phi_S^p(r,y) \tag{5}$$

where ϕ_D^p, ϕ_I^p, and ϕ_S^p are diffraction, incident, and scattering potentials, and ϕ_{Rj}^p denotes the radiation potential corresponding to the jth mode for each pth mode, respectively. From now on, we set the incident wave amplitude A to be unity for convenience. The incident wave potential ϕ_I^p is given by

$$\phi_I^p(r,y)=\beta_p J_p(k_1r)\frac{\cosh k_1(y+h)}{\cosh k_1h} \tag{6}$$

where k_1 is the wave number for progressive waves and satisfies $\omega^2=gk_1\tanh k_1h$ with g being the gravitational acceleration. The symbol β_p=1, when p=0, and $\beta_p=2(i)^p$, when $p\geq 1$.

2.1 Diffraction Problem

In this section, we first consider the diffraction of incident waves by a rigid horizontal disk. The scattering potential ϕ_s^p satisfies

$$\left(\frac{\partial^2}{\partial r^2}+\frac{1}{r}\frac{\partial}{\partial r}+\frac{\partial^2}{\partial y^2}-\frac{p^2}{r^2}\right)\phi_S^p=0\ ,p=0,1,2,\ldots \text{ in the fluid domain} \tag{7}$$

with the following boundary conditions

$$\frac{\partial\phi_S^p}{\partial y}-\nu\phi_S^p=0 \text{ on } y=0\ \left(\nu=\frac{\omega^2}{g}\right) \tag{8}$$

$$\frac{\partial\phi_S^p}{\partial y}=0 \text{ on } y=-h \tag{9}$$

$$\frac{\partial\phi_S^p}{\partial y}=0 \text{ on } y=-d,\ |r|\leq a \tag{10}$$

and

$$(k_1r)^{1/2}\left(\frac{\partial}{\partial r}-ik_1\right)\phi_S^p\to 0 \text{ as } k_1r\to\infty \tag{11}$$

The fluid domain is divided into three regions as shown in Fig. 1, i.e., (I) the exterior region outside the disk ($|r|\geq a$, $-h\leq y\leq 0$); (II) the interior region above the disk ($|r|\leq a$, $-d\leq y\leq 0$); (III) the interior region below the disk ($|r|\leq a$, $-h\leq y\leq -d$).

By using separation of variables and applying above boundary conditions, we can obtain the general expression of ϕ_D^p in the three subregions:

$$\phi_D^{p(1)}=[\beta_pJ_p(k_1r)+c_{p0}H_p(k_1r)]f_{10}(y)+\sum_{n=1}^{\infty}c_{pn}K_p(k_{1n}r)f_{1n}(y) \tag{12}$$

$$\phi_D^{p(2)}=a_{p0}J_p(k_2r)f_{20}(y)+\sum_{n=1}^{\infty}a_{pn}I_p(k_{2n}r)f_{2n}(y) \tag{13}$$

$$\phi_D^{p(3)}=b_{p0}\left(\frac{r}{a}\right)^pf_{30}(y)+\sum_{n=1}^{\infty}b_{pn}I_p(k_{3n}r)f_{3n}(y) \tag{14}$$

where J_p and Y_p are the Bessel functions of the first and second kind of order p; H_p is the Hankel function of the first kind of order p; I_p and K_p are the modified Bessel functions of the first and second kind, respectively, of order p.

The eigenfunctions $f_{1n}(y)$, $f_{2n}(y)$ and $f_{3n}(y)$ are then given by

$$f_{1n}(y)=\begin{cases}\dfrac{\cosh k_1(y+h)}{\cosh k_1h}, & n=0\\ \dfrac{\cos k_{1n}(y+h)}{\cos k_{1n}h}, & n\geq 1\end{cases} \tag{15}$$

$$f_{2n}(y)=\begin{cases}\dfrac{\cosh k_2(y+d)}{\cosh k_2d}, & n=0\\ \dfrac{\cos k_{2n}(y+d)}{\cos k_{2n}d}, & n\geq 1\end{cases} \tag{16}$$

$$f_{3n}(y)=\frac{\cos k_{3n}(y+h)}{\cos k_{3n}(h-d)},\ n\geq 0 \tag{17}$$

The corresponding eigenvalues k_{1n}, k_{2n}, k_{3n} are the solutions of the following equations:

$$\begin{cases} k_1\tanh k_1 h=\dfrac{\omega^2}{g},\ n=0 \\ k_{1n}\tan k_{1n}h=-\dfrac{\omega^2}{g},\ n\geq 1 \end{cases} \tag{18}$$

$$\begin{cases} k_2\tanh k_2 d=\dfrac{\omega^2}{g},\ n=0 \\ k_{2n}\tan k_{2n}d=-\dfrac{\omega^2}{g},\ n\geq 1 \end{cases} \tag{19}$$

$$k_{3n}=\frac{n\pi}{(h-d)},\ n\geq 0 \tag{20}$$

The unknown coefficients $a_{pn}, b_{pn}, c_{pn} (p,n=0,1,2,\ldots)$, are determined by invoking continuity of pressure and radial velocity on $r=a$. The continuity of ϕ_D^p on $r=a$ requires

$$[\beta_p J_p(k_1 a)+c_{p0}H_p(k_1 a)]f_{10}(y) + \sum_{n=1}^{\infty} c_{pn}K_p(k_{1n}a)f_{1n}(y) \tag{21a}$$

$$=\begin{cases} a_{p0}J_p(k_2 a)f_{20}(y)+\sum_{n=1}^{\infty} a_{pn}I_p(k_{2n}a)f_{2n}(y),\ -d\leq y\leq 0 \\ b_{p0}f_{30}(y)+\sum_{n=1}^{\infty} b_{pn}I_p(k_{3n}a)f_{3n}(y),\ -h\leq y\leq -d \end{cases} \tag{21b}$$

Multiplying (21a) by the orthogonal eigenfuction $f_{2l}(y)$ and integrating over $[-d, 0]$, we obtain

$$[\beta_p J_p(k_1 a)+c_{p0}H_p(k_1 a)]\Gamma_{l0}+\sum_{n=1}^{\infty} c_{pn}K_p(k_{1n}a)\Gamma_{ln} =\begin{cases} a_{p0}J_p(k_2 a)N_0^{(2)}, l=0 \\ a_{pl}I_p(k_{2l}a)N_l^{(2)}, l\geq 1 \end{cases} \tag{22}$$

where

$$\Gamma_{ln}=\int_{-d}^{0} f_{1n}(y)f_{2l}(y)dy$$

$$\int_{-d}^{0} f_{2n}(y)f_{2l}(y)dy=\begin{cases} N_l^{(2)}, l=n \\ 0, \quad l\neq n \end{cases}$$

Similarly, by multiplying (21b) by $f_{3l}(y)$ and integrating with respect to y from $-h$ to $-d$, the following equation can be obtained:

$$[\beta_p J_p(k_1 a)+c_{p0}H_p(k_1 a)]\Lambda_{l0}+\sum_{n=1}^{\infty} c_{pn}K_p(k_{1n}a)\Lambda_{ln} =\begin{cases} b_{p0}N_0^{(3)}, l=0 \\ b_{pl}I_p(k_{3l}a)N_l^{(3)}, l\geq 1 \end{cases} \tag{23}$$

where

$$\Lambda_{ln}=\int_{-h}^{-d} f_{1n}(y)f_{3l}(y)dy$$

$$\int_{-h}^{-d} f_{3n}(y)f_{3l}(y)dy=\begin{cases} N_l^{(3)}, l=n \\ 0, \quad l\neq n \end{cases}$$

The continuity of $\partial\phi_D^p/\partial r$ on $r=a$ gives

$$k_1[\beta_p J_p'(k_1 a)+c_{p0}H_p'(k_1 a)]f_{10}(y) + \sum_{n=1}^{\infty} c_{pn}k_{1n}K_p'(k_{1n}a)f_{1n}(y)$$

$$=\begin{cases} a_{p0}k_2 J_p'(k_2 a)f_{20}(y)+\sum_{n=1}^{\infty} a_{pn}k_{2n}I_p'(k_{2n}a)f_{2n}(y),\ -d\leq y\leq 0 \\ \left(\dfrac{p}{a}\right)b_{p0}f_{30}(y)+\sum_{n=1}^{\infty} b_{pn}k_{3n}I_p'(k_{3n}a)f_{3n}(y),\ -h\leq y\leq -d \end{cases} \tag{24}$$

where $J_p'(k_1 a)=dJ_p(k_1 r)/d(k_1 r)|_{r=a}$, etc

By multiplying both sides of Eq. (24) by $f_{1l}(y)$ and integrating with respect to y from $-h$ to 0, we obtain

$$k_1[\beta_p J_p'(k_1 a)+c_{p0}H_p'(k_1 a)]N_0^{(1)}=a_{p0}k_2 J_p'(k_2 a)\Gamma_{00} + \sum_{n=1}^{\infty} a_{pn}k_{2n}I_p'(k_{2n}a)\Gamma_{n0}+\left(\frac{p}{a}\right)b_{p0}\Lambda_{00} + \sum_{n=1}^{\infty} b_{pn}k_{3n}I_p'(k_{3n}a)\Lambda_{n0},\ l=0$$

$$c_{pl}k_{1l}K_p'(k_{1l}a)N_l^{(1)}=a_{p0}k_2 J_p'(k_2 a)\Gamma_{0l} + \sum_{n=1}^{\infty} a_{pn}k_{2n}I_p'(k_{2n}a)\Gamma_{nl}+\left(\frac{p}{a}\right)b_{p0}\Lambda_{0l} + \sum_{n=1}^{\infty} b_{pn}k_{3n}I_p'(k_{3n}a)\Lambda_{nl},\ l\geq 1 \tag{25}$$

where

$$\int_{-h}^{0} f_{1n}(y)f_{1l}(y)dy=\begin{cases} N_l^{(1)}, l=n \\ 0, \quad l\neq n \end{cases}$$

The final matrix equation can be obtained after substituting Eqs. (22) and (23) into (25):

$$c_{p0}+\sum_{k=0}^{\infty}\frac{F_{0k}}{k_1 N_0^{(1)}H_p'(k_1 a)}c_{pk}=\frac{X_{p0}}{k_1 N_0^{(1)}H_p'(k_1 a)},\ l=0$$

$$c_{pl}+\sum_{k=0}^{\infty}\frac{F_{lk}}{k_{1l}N_l^{(1)}K_p'(k_{1l}a)}c_{pk}=\frac{X_{pl}}{k_{1l}N_l^{(1)}K_p'(k_{1l}a)},\quad l\geq 1 \tag{26}$$

where

$$F_{l0}=$$

$$-\frac{k_2H_p(k_1a)J_p'(k_2a)\Gamma_{00}\Gamma_{0l}}{J_p(k_2a)N_0^{(2)}}-\sum_{n=1}^{\infty}\frac{k_{2n}H_p(k_1a)I_p'(k_{2n}a)\Gamma_{n0}\Gamma_{nl}}{I_p(k_{2n}a)N_n^{(2)}}$$

$$-\left(\frac{p}{a}\right)\frac{H_p(k_1a)\Lambda_{00}\Lambda_{0l}}{N_0^{(3)}}-\sum_{n=1}^{\infty}\frac{k_{3n}H_p(k_1a)I_p'(k_{3n}a)\Lambda_{n0}\Lambda_{nl}}{I_p(k_{3n}a)N_n^{(3)}}$$

$$F_{lk}=$$

$$-\frac{k_2K_p(k_{1k}a)J_p'(k_2a)\Gamma_{0k}\Gamma_{0l}}{J_p(k_2a)N_0^{(2)}}-\sum_{n=1}^{\infty}\frac{k_{2n}K_p(k_{1k}a)I_p'(k_{2n}a)\Gamma_{nk}\Gamma_{nl}}{I_p(k_{2n}a)N_n^{(2)}}$$

$$-\left(\frac{p}{a}\right)\frac{K_p(k_{1k}a)\Lambda_{0k}\Lambda_{0l}}{N_0^{(3)}}-\sum_{n=1}^{\infty}\frac{k_{3n}K_p(k_{1k}a)I_p'(k_{3n}a)\Lambda_{nk}\Lambda_{nl}}{I_p(k_{3n}a)N_n^{(3)}}$$

$$X_{pl}=$$

$$-\frac{k_2\beta_pJ_p(k_1a)J_p'(k_2a)\Gamma_{00}\Gamma_{0l}}{J_p(k_2a)N_0^{(2)}}-\sum_{n=1}^{\infty}\frac{k_{2n}\beta_pJ_p(k_1a)I_p'(k_{2n}a)\Gamma_{n0}\Gamma_{nl}}{I_p(k_{2n}a)N_n^{(2)}}$$

$$+\left(\frac{p}{a}\right)\frac{\beta_pJ_p(k_1a)\Lambda_{00}\Lambda_{0l}}{N_0^{(3)}}+\sum_{n=1}^{\infty}\frac{k_{3n}\beta_pJ_p(k_1a)I_p'(k_{3n}a)\Lambda_{n0}\Lambda_{nl}}{I_p(k_{3n}a)N_n^{(3)}}$$

$$-k_1\beta_pJ_p'(k_1a)N_0^{(1)}\delta_{l0}$$

For each fixed p, the above equations constitute a linear simultaneous algebraic equation in terms of the unknown constants c_{pl} (l=0,1,2,...). For numerical solutions of Eq. (26), we truncate the series after N-th term. Thus, we have (N+1) unknowns of c_{pk}. The unknown constants a_{pl}, b_{pl} (l=0,1,2,...N) for regions II and III can be easily evaluated using the following equations derived from Eqs. (22) and (23):

$$a_{p0}=\frac{[\beta_pJ_p(k_1a)+c_{p0}H_p(k_1a)]\Gamma_{00}+\sum_{k=1}^{N}c_{pk}K_p(k_{1k}a)\Gamma_{0k}}{J_p(k_2a)N_0^{(2)}},\quad l=0$$

$$a_{pl}=\frac{[\beta_pJ_p(k_1a)+c_{p0}H_p(k_1a)]\Gamma_{l0}+\sum_{k=1}^{N}c_{pk}K_p(k_{1k}a)\Gamma_{lk}}{I_p(k_{2l}a)N_l^{(2)}},\quad l\geq 1$$

$$b_{p0}=\frac{[\beta_pJ_p(k_1a)+c_{p0}H_p(k_1a)]\Lambda_{00}+\sum_{k=1}^{N}c_{pk}K_p(k_{1k}a)\Lambda_{0k}}{N_0^{(3)}},\quad l=0$$

$$b_{pl}=\frac{[\beta_pJ_p(k_1a)+c_{p0}H_p(k_1a)]\Lambda_{l0}+\sum_{k=1}^{N}c_{pk}K_p(k_{1k}a)\Lambda_{lk}}{I_p(k_{3l}a)N_l^{(3)}},\quad l\geq 1 \tag{27}$$

2.2 Radiation Problem

In this section, we study the generation of outgoing waves due to the elastic response of a flexible-membrane disk of negligible thickness. The boundary-value problem for the radiation potential is the same as that of scattering potential (Eqs. 7-11) except the following body boundary condition.

$$\frac{\partial\phi_{Rj}^{p}}{\partial y}=-i\omega\xi \text{ on } y=-d,|r|\leq a \tag{28}$$

The radiation potentials in each region can be expressed as follows

$$\phi_{Rj}^{p(1)}=c_{p0}^{j}H_p(k_1r)f_{10}(y)+\sum_{n=1}^{\infty}c_{pn}^{j}K_p(k_{1n}r)f_{1n}(y) \tag{29}$$

$$\phi_{Rj}^{p(2)}=a_{p0}^{j}J_p(k_2r)f_{20}(y)+\sum_{n=1}^{\infty}a_{pn}^{j}I_p(k_{2n}r)f_{2n}(y)+\frac{i\omega}{g}\tilde{\phi}_{Rj}^{p(2)}(r,y) \tag{30}$$

$$\phi_{Rj}^{p(3)}=b_{p0}^{j}\left(\frac{r}{a}\right)^{p}f_{30}(y)+\sum_{n=1}^{\infty}b_{pn}^{j}I_p(k_{3n}r)f_{3n}(y)+\frac{i\omega}{g}\tilde{\phi}_{Rj}^{p(3)}(r,y) \tag{31}$$

In particular, the radiation potentials in regions II and III can be expressed by the sum of homogeneous solutions and particular solutions. The homogeneous solutions satisfy the zero-normal-velocity condition on the disk surface, while the particular solutions $\tilde{\phi}_{Rj}^{p}$ satisfy the following body boundary condition there:

$$\frac{\partial\tilde{\phi}_{Rj}^{p}}{\partial y}=-i\omega J_p(\Omega_{pj}r/a) \text{ on } y=-d,|r|\leq a \tag{32}$$

The particular solutions in regions (II) and (III) can be obtained by the method of separation of variables:

$$\tilde{\phi}_{Rj}^{p(2)}(r,y)=$$

$$\frac{-i\omega J_p(\Omega_{pj}r/a)[(\Omega_{pj}/a)\cosh(\Omega_{pj}y/a)+\nu\sinh(\Omega_{pj}y/a)]}{(\Omega_{pj}/a)[-(\Omega_{pj}/a)\sinh(\Omega_{pj}d/a)+\nu\cosh(\Omega_{pj}d/a)]} \tag{33}$$

$$\tilde{\phi}_{Rj}^{p(3)}(r,y)=\frac{-i\omega J_p(\Omega_{pj}r/a)\cosh[\Omega_{pj}(y+h)/a]}{(\Omega_{pj}/a)\sinh[\Omega_{pj}(h-d)/a]} \tag{34}$$

We next apply the matching conditions (the continuity of velocity potential and its normal derivative) to solve for the unknown constants in each region. The matching conditions to be satisfied at r=a are

$$\phi_{Rj}^{p(1)}=\begin{cases}\phi_{Rj}^{p(2)}, & -d\le y\le 0\\ \phi_{Rj}^{p(3)}, & -h\le y\le -d\end{cases}\qquad \frac{\partial\phi_{Rj}^{p(1)}}{\partial r}=\begin{cases}\dfrac{\partial\phi_{Rj}^{p(2)}}{\partial r}, & -d\le y\le 0\\ \dfrac{\partial\phi_{Rj}^{p(3)}}{\partial r}, & -h\le y\le -d\end{cases} \tag{35}$$

By following the same procedure, as in the diffraction problem, we finally obtain algebraic equations for the unknown constants $c_{pl}^{j}(l=0,1,2,3,\ldots N)$ for each fixed p:

$$c_{pl}^{j}+\sum_{k=0}^{N}\frac{F_{lk}}{k_{1l}N_l^{(1)}K_p'(k_{1l}a)}c_{pk}^{j}=\frac{X_{pl}^{j}}{k_{1l}N_l^{(1)}K_p'(k_{1l}a)},\quad l=0,1,2,3\ldots N \tag{36}$$

where

$$X_{pl}^{j}=\frac{i\omega}{g}\left\{\int_{-d}^{0}\frac{\partial\tilde{\phi}_{Rj}^{p(2)}(a,y)}{\partial r}f_{1l}(y)dy+\int_{-h}^{-d}\frac{\partial\tilde{\phi}_{Rj}^{p(3)}(a,y)}{\partial r}f_{1l}(y)dy\right\} \tag{37}$$

The other unknown coefficients can be determined from

$$a_{po}^{j}=$$

$$\frac{c_{p0}^{j}H_p(k_1a)\Gamma_{00}+\sum_{k=1}^{N}c_{pk}^{j}K_p(k_{1k}a)\Gamma_{0k}-\frac{i\omega}{g}\int_{-d}^{0}\tilde{\phi}_{Rj}^{p(2)}(a,y)f_{20}(y)dy}{J_p(k_2a)N_0^{(2)}},$$

$l=0$

$$a_{pl}^{j}=$$

$$\frac{c_{p0}^{j}H_p(k_1a)\Gamma_{l0}+\sum_{k=1}^{N}c_{pk}^{j}K_p(k_{1k}a)\Gamma_{lk}-\frac{i\omega}{g}\int_{-d}^{0}\tilde{\phi}_{Rj}^{p(2)}(a,y)f_{2l}(y)dy}{I_p(k_{2l}a)N_l^{(2)}},$$

$l\ge 1$

$$b_{p0}^{j}=$$

$$\frac{c_{p0}^{j}H_p(k_1a)\Lambda_{00}+\sum_{k=1}^{N}c_{pk}^{j}K_p(k_{1k}a)\Lambda_{0k}-\frac{i\omega}{g}\int_{-h}^{-d}\tilde{\phi}_{Rj}^{p(3)}(a,y)f_{30}(y)dy}{N_0^{(3)}},$$

$l=0$

$$b_{pl}^{j}=$$

$$\frac{c_{p0}^{j}H_p(k_1a)\Lambda_{l0}+\sum_{k=1}^{N}c_{pk}^{j}K_p(k_{1k}a)\Lambda_{lk}-\frac{i\omega}{g}\int_{-h}^{-d}\tilde{\phi}_{Rj}^{p(3)}(a,y)f_{3l}(y)dy}{I_p(k_{3l}a)N_l^{(3)}},$$

$l\ge 1$ (38)

2.3 Membrane Responses

The motion of circular membrane is governed by the linearized membrane equation

$$T\left(\frac{\partial^2\xi}{\partial r^2}+\frac{1}{r}\frac{\partial\xi}{\partial r}+\frac{1}{r^2}\frac{\partial^2\xi}{\partial\theta^2}\right)+m\omega^2\xi$$

$$=-i\rho\omega[\phi^{(3)}(r,\theta,-d)-\phi^{(2)}(r,\theta,-d)] \tag{39}$$

where m is the mass per unit area. Substituting Eqs. (2) and (5) into (39), the equation of motion can be rewritten as follows:

$$\sum_{p=0}^{\infty}\sum_{j=1}^{\infty}\varsigma_{pj}\left\{\left[-T\frac{\partial^2}{\partial r^2}-\frac{T}{r}\frac{\partial}{\partial r}-\frac{T}{r^2}\frac{\partial^2}{\partial\theta^2}-m\omega^2\right]w_{pj}(r,\theta)-p_{Rj}(r,\theta)\right\}$$

$$=\sum_{p=0}^{\infty}p_D(r,\theta) \tag{40}$$

where

$$p_{Rj}(r,\theta)=\rho g[\phi_{Rj}^{p(3)}(r,-d)-\phi_{Rj}^{p(2)}(r,-d)]\cos p\theta$$

$$p_D(r,\theta)=\rho g[\phi_D^{p(3)}(r,-d)-\phi_D^{p(2)}(r,-d)]\cos p\theta \tag{41}$$

Multiplying Eq. (40) by $w_{qi}(r,\theta)$ and integrating over the entire area of disk, we obtain the equation of motion of circular membrane in the form

$$\sum_{j=1}^{\infty}\{K_{ij}-\omega^2(M_{ij}+a_{ij})-i\omega b_{ij}\}\varsigma_{qj}=F_i, i=1,2,\ldots,\ q=0,1,2,\ldots \tag{42}$$

where

$$K_{ij}=\begin{cases}T(1+\delta_{q0})\pi\left(\dfrac{\Omega_{qi}}{a}\right)^2N_{qi}, & i=j\\ 0, & i\ne j\end{cases} \tag{43a}$$

$$M_{ij}=\begin{cases}m(1+\delta_{q0})\pi N_{qi}, & i=j\\ 0, & i\ne j\end{cases} \tag{43b}$$

$$a_{ij}=\sum_{p=0}^{\infty}\Re\left\{\frac{1}{\omega^2}\int_0^{2\pi}\int_0^a p_{Rj}(r,\theta)rw_{qi}(r,\theta)drd\theta\right\}$$

$$=\rho g\pi(1+\delta_{q0})\Re\left\{\frac{1}{\omega^2}\int_0^a r(\phi_{Rj}^{q(3)}-\phi_{Rj}^{q(2)})|_{y=-d}J_p\left(\frac{\Omega_{qi}}{a}r\right)dr\right\} \tag{43c}$$

$$b_{ij}=\sum_{p=0}^{\infty}\Im\left\{\frac{1}{\omega}\int_0^{2\pi}\int_0^a p_{Rj}(r,\theta)rw_{qi}(r,\theta)drd\theta\right\}$$

$$=\rho g\pi(1+\delta_{q0})\Im\left\{\frac{1}{\omega}\int_0^a r(\phi_{Rj}^{q(3)}-\phi_{Rj}^{q(2)})|_{y=-d}J_p\left(\frac{\Omega_{qi}}{a}r\right)dr\right\} \tag{43d}$$

$$F_i=\sum_{p=0}^{\infty}\int_0^{2\pi}\int_0^a p_D(r,\theta)rw_{qi}(r,\theta)drd\theta$$

$$=\rho g\pi(1+\delta_{q0})\left\{\int_0^a r(\phi_D^{q(3)}-\phi_D^{q(2)})|_{y=-d}J_p\left(\frac{\Omega_{qi}}{a}r\right)dr\right\} \tag{43e}$$

where K_{ij}, M_{ij}, and F_i are the generalized stiffness matrix, mass matrix, and force vector, respectively, and a_{ij} and b_{ij} are the generalized added-mass and damping matrices. Truncating the series in Eq. (42) at the appropriate term N_r and solving for q=0,1,2....N_θ, we can determine the unknown complex amplitudes corresponding to each mode (q, j).

The hydrodynamic force acting on a flexible disk can be obtained by integrating the hydrodynamic pressure over the disk area.

$$F=i\omega\rho\int_0^{2\pi}\int_0^a r(\phi^{(3)}-\phi^{(2)})|_{y=-d}drd\theta \tag{44}$$

Substituting Eq. (5) into the above equation and integrating with respect to θ, the hydrodynamic force can be expressed in terms of diffraction and radiation parts.

$$F=F_D+\sum_{j=1}^{N_r}\varsigma_{0j}F_{Rj} \tag{45}$$

where

$$F_D=2\pi\rho g\int_0^a r(\phi_D^{0(3)}-\phi_D^{0(2)})|_{y=-d}dr$$

$$F_{Rj}=2\pi\rho g\int_0^a r(\phi_{Rj}^{0(3)}-\phi_{Rj}^{0(2)})|_{y=-d}dr \tag{46}$$

3. NUMERICAL RESULTS AND DISCUSSIONS

In this section, the analytic solutions derived in the preceding sections are used to investigate the diffraction/radiation wave field in the neighborhood of a submerged circular flexible membrane for various design and wave conditions. First,. the convergence of analytic solutions with the number of natural modes (N_θ, N_r) for given N is shown in Table 1 for a particular design condition. The convergence is in general rapid with respect to the two parameters. Through a series of similar tests, it is concluded that (N_θ, N_r)=(6,5) gives sufficient accuracy for the cases presented here. Second, the convergence test of analytic solutions with the number of eigenfunctions N for given (N_θ, N_r)=(6,5) is shown in Fig. 2. It is found that N=15 is sufficient to give the reasonable results. In the following, the analytic solutions with N_θ=6, N_r=5, N=15 were used to investigate the wave deformation over a submerged flexible circular disk for various design conditions. The membrane mass per unit area used for these numerical examples was 1.0 kg/m^2.

Fig. 3 shows the diffracted wave amplitude normalized

Table 1. Convergence test results ($|\eta|/A$) with the number of natural modes (N_θ, N_r) for d/h=0.2, a/h=0.5, N=15, $T/\rho gh^2$=0.05 at θ=0, $r=a$

(a) k_1h=2.0

N_r \ N_θ	0	2	4	6	8
1	0.265130	0.825257	0.785191	0.785694	0.785691
3	0.255252	0.826043	0.785975	0.786478	0.786475
5	0.265261	0.826065	0.785998	0.786501	0.786498
7	0.265262	0.826068	0.786001	0.786504	0.786501

(a) k_1h=2.0

N_r \ N_θ	0	2	4	6	8
1	0.450707	1.37881	1.23184	1.23726	1.23714
3	0.451324	1.37953	1.23339	1.23876	1.23864
5	0.451329	1.37958	1.23347	1.23884	1.23872
7	0.451329	1.37959	1.23349	1.23885	1.23873

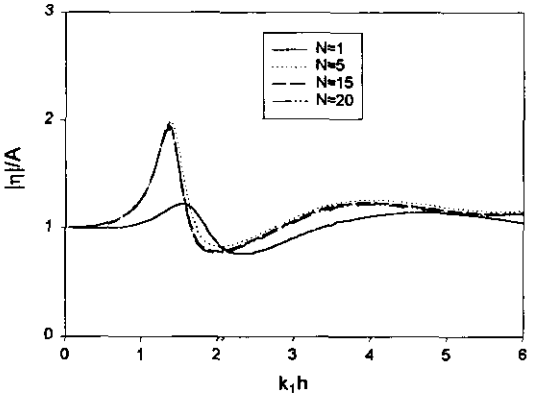

Fig. 2. Convergence of wave height at $r=a$,θ=0 with the number of eigenfunctions for the case a/h=0.5, $T/\rho gh^2$=0.05, d/h=0.2.

by incident wave amplitude for a rigid (=infinite tension) circular disk at three locations $r=a$, θ=0, π/2,π. In this figure, the relative radius of the disk, a/h, is fixed at 0.5 and three different relative submerged depths, d/h=0.1,0.2, and 0.3, are used. The present results are in good agreement with the published data of Yu and Chwang (1993). It is shown that the effects of disk on the diffracted wave field increase as the submerged depth of disk decreases. When θ=0 and d/h=0.1, the water surface continues to rise in an oscillatory manner as k_1h increases, which implies that the shorter the wavelength, the more wave energy is focused near the rear of the shallow disk. As k_1h approaches 0

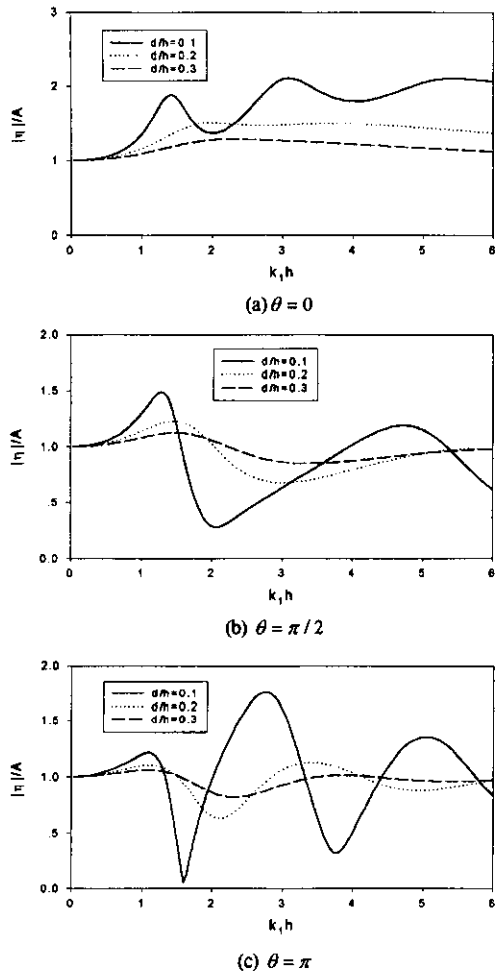

Fig. 3. Variation of wave height due to rigid disk as function of non-dimensional submergence depth d/h and wave-number k_1h for a/h=0.5 at r=a.

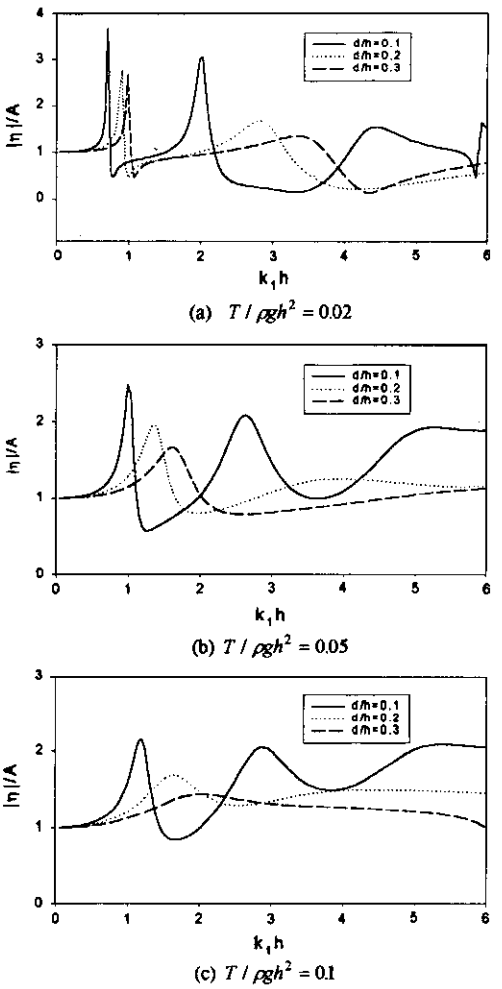

Fig. 4. Variation of wave height due to flexible disk as function of non-dimensional submergence depth d/h and wave-number k_1h for a/h=0.5 at r=a, θ=0.

(long wave limit), all curves converge toward 1, which means that the incident wave field is not changed.

Figs. 4 and 5 show the variation of wave amplitude due to the flexible disk for three different tensions and submerged depths at r=a, θ=0, π. When the tension is not large, the membrane becomes flexible and the resulting free-surface elevation is quite different from that of the rigid-disk case. As the membrane tension increases, the results become closer to the rigid-disk results. When the non-dimensional tension is 0.02, very pronounced wave focusing (three or four times the incident wave amplitude) is possible in a very narrow frequency region. This is due to the reinforcement of diffracted waves by motion-induced waves. The pattern of motion-induced waves is closely dependent to the tension and submerged depth. The effects of membrane motions are more pronounced as the submergence depth is reduced and the flexibility increases.

To investigate the effect of membrane tension more clearly, the free-surface elevations at three different locations, r=a, θ=0, π/2,π, are plotted in Fig. 6 for four different tensions and the fixed value of d/h=0.2, a/h=0.5. In these figures, solid lines denote the cases of infinity tension (or rigid disk). It is shown that the curves converge toward the rigid-disk case, as membrane tension increases. Fig. 7 shows the effects of disk size for fixed sub-

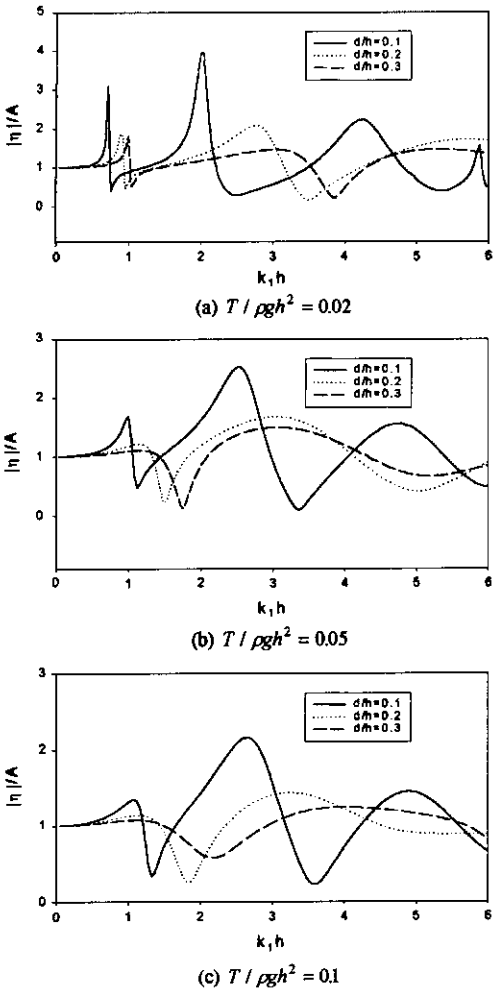

Fig. 5. Variation of wave height due to flexible disk as function of non-dimensional submergence depth d/h and wavenumber k_1h for a/h=0.5 at r=a, θ=π.

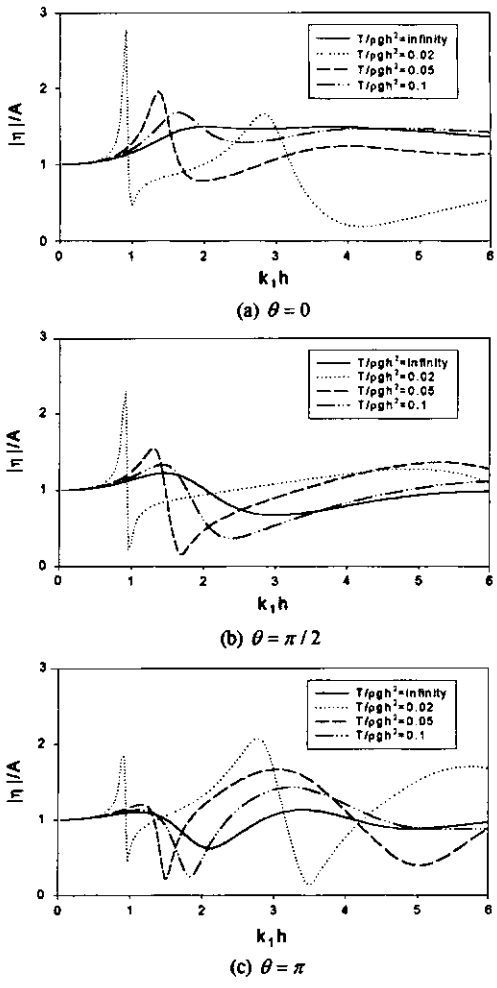

Fig. 6. Variation of wave height due to flexible disk as function of non-dimensional tension $T/\rho gh^2$ and wavenumber k_1h for a/h=0.5, d/h=0.2 at r=a.

mergence depth and tension. As the size increases, sharper wave focusing occurs at lower frequencies. The shift of focusing frequency is due to the change of modal response frequencies.

In Figs. 8 and 9, dimensionless hydrodynamic forces on the rigid and flexible disks are plotted as function of k_1h. The forces on the flexible membrane is in general greater than those on the rigid disk due to additional hydrodynamic loading induced by membrane motions. The peak-force magnitude increases as submergence decreases. As the wavenumber k_1h increases, the hydrodynamic loading on a shallower flexible disk can be smaller, as shown in Fig. 9. Fig. 10 shows the variation of dimensionless hydrodynamic forces with membrane tension for fixed d/h=0.2. It is clearly seen that large tension cases approach the rigid-disk limit and the peak magnitudes tend to be higher and sharper as membrane flexibility increases. Fig. 11 describes the variation of dimensionless hydrodynamic forces according to the change of disk size (a/h=0.3, 0.4, 0.5) for d/h=0.2, $T/\rho gh^2$=0.05. It is shown that the peak magnitude increases and the width of the peak decrease as disk size increases. It shows the similar pattern as Fig. 10. It can be explained that the larger the disk has an effect to increase the flexibility of membrane.

Fig. 12 compares the deformation of incident wave field around the rigid and flexible disks for d/h=0.2, $a/$

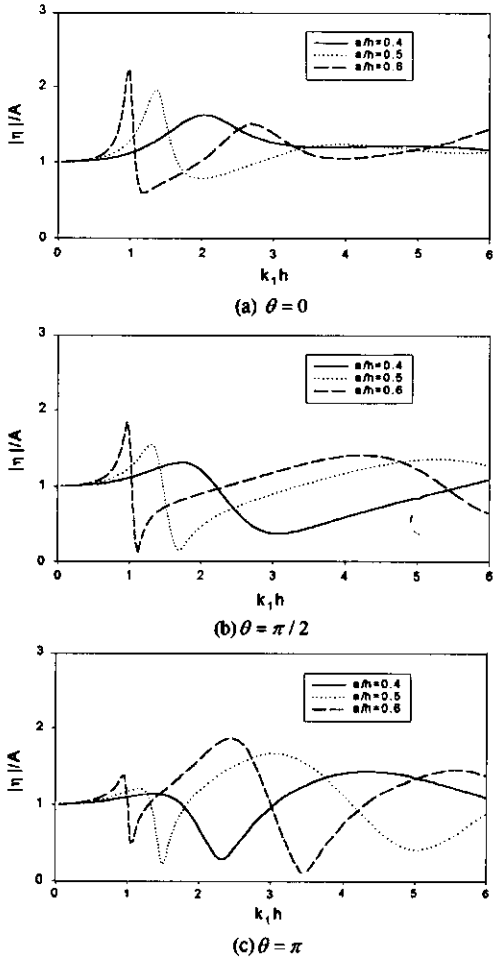

Fig. 7. Variation of wave height due to flexible disk as function of non-dimensional radius of disk a/h and wavenumber k_1h for $T/\rho gh^2$=0.05, d/h=0.2 at r=a.

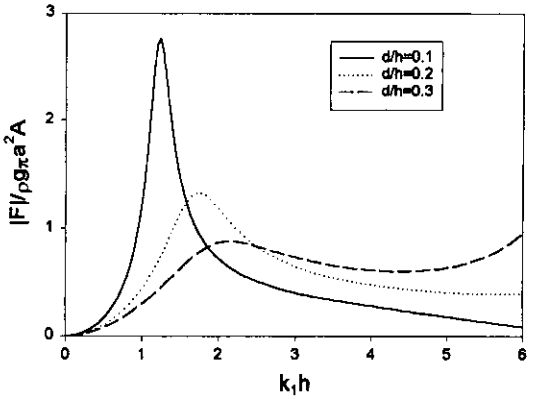

Fig. 9. Hydrodynamic force acting on a flexible disk as function of non-dimensional submergence depth d/h and wavenumber k_1h for a/h=0.5, $T/\rho gh^2$=0.1.

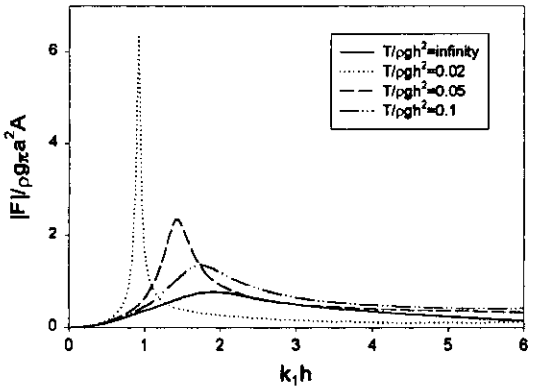

Fig. 10. Hydrodynamic force acting on a flexible disk as function of non-dimensional tension $T/\rho gh^2$ and wavenumber k_1h for a/h=0.5, d/h=0.2.

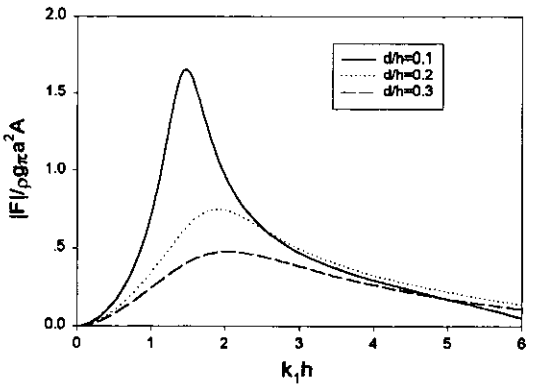

Fig. 8. Hydrodynamic force acting on a rigid disk as function of non-dimensional submergence depth d/h and wavenumber k_1h for a/h=0.5.

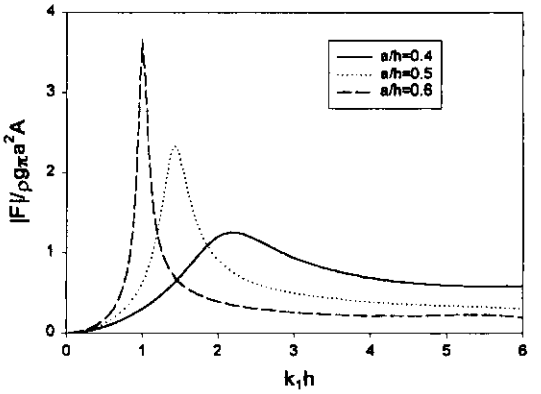

Fig. 11. Hydrodynamic force acting on a flexible disk as function of non-dimensional radius of disk a/h and wavenumber k_1h for $T/\rho gh^2$=0.05, d/h=0.2.

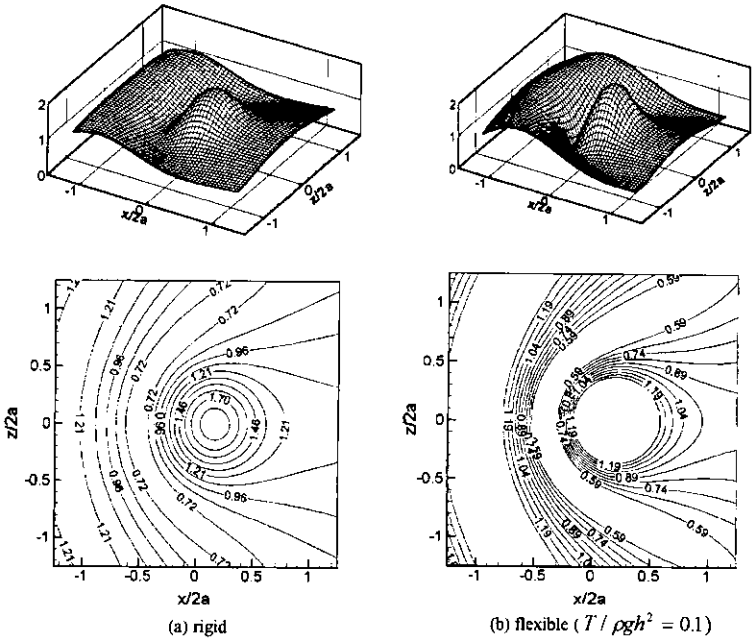

Fig. 12. Comparison of wave deformation ($|\eta|/A$) around submerged disks for d/h=0.2, a/h=0.5 at k_1h=2.0.

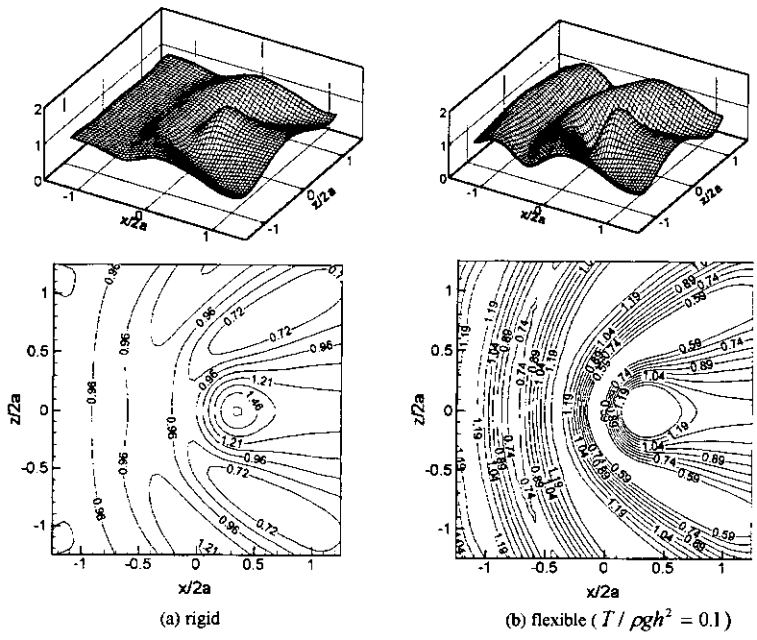

Fig. 13. Comparison of wave deformation ($|\eta|/A$) around submerged disks for d/h=0.2, a/h=0.5 at k_1h=4.0.

h=0.5, k_1h=2.0. In these figures, we can observe wave focusing near the rear of the disk, and the focusing rate is greater in the case of flexible one, which shows that wave focusing rate or locations can be varied by controlling membrane flexibility. The wave focusing results from the phase reinforcement between diffracted and motion-in-

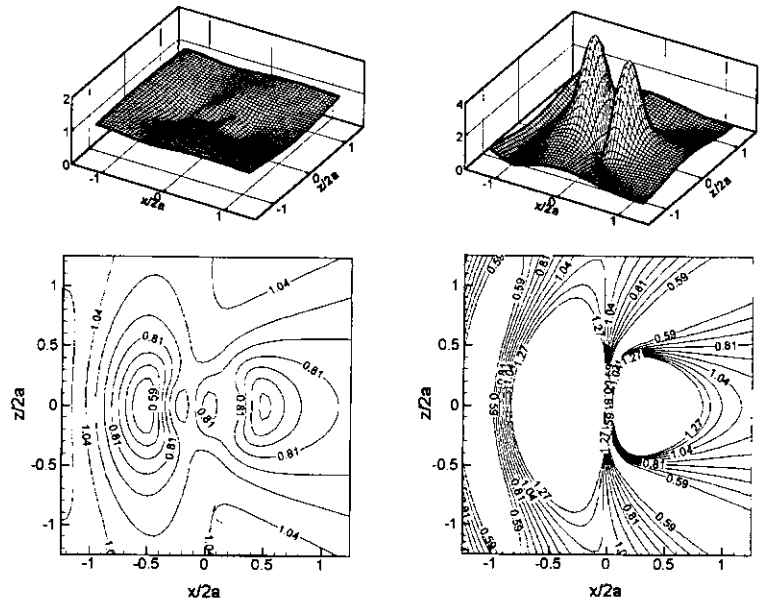

(a) $T / \rho g h^2 = 0.01$ (b) $T / \rho g h^2 = 0.02$

Fig. 14. Comparison of wave deformation ($|\eta|/A$) around submerged flexible disks for d/h=0.1, a/h=0.5 at k_1h=2.0.

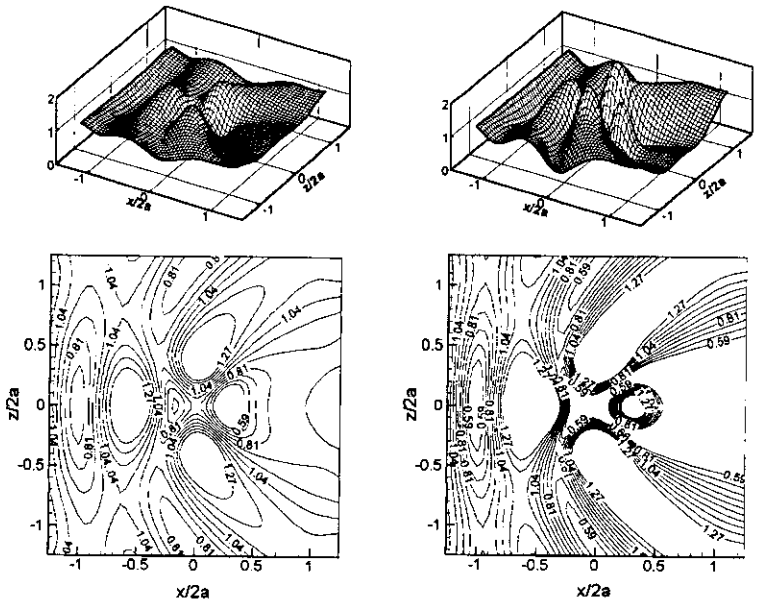

(a) $T / \rho g h^2 = 0.01$ (b) $T / \rho g h^2 = 0.02$

Fig. 15. Comparison of wave deformation ($|\eta|/A$) around submerged flexible disks for d/h=0.1, a/h=0.5 at k_1h=4.0.

duced waves. Fig. 13 shows similar comparison for larger water depth to wavelength ratio k_1h=4. In this case, wave focusing occurs at several locations instead of a single peak, and its pattern becomes more complicated compared to the previous case.

Fig. 14 shows another example of wave deformation by

a flexible membrane with two different tensions for d/h=0.1, and k_1h=2. When the dimensionless tension is 0.01, the free surface above the membrane disk becomes lower than the incident wave field as a result of phase cancellation. On the other hand, for higher tension (dimensionless tension=0.02), the free-surface pattern becomes totally different, and two pronounced peaks can be observed. Fig. 15 shows how the free-surface pattern of Fig. 14 changes if the wavelength is halved. For dimensionless tension=0.01, we again see depressions on the free surface above the circular membrane. In the case of dimensionless tension=0.02, four peaks are formed above the membrane as a result of higher-mode membrane responses.

Various types of membrane responses are illustrated in Fig. 16 for d/h=0.1, 0.2, k_1h=2,4,6, and non-dimensional tension=0.02. It is seen that various shapes of membrane responses can be generated depending on wave and membrane parameters. Particularly for shallower submerged depth, many interesting patterns, such as two-peak, four-peak, and sombrero shapes, are made. For each case, the shape is determined by which mode is dominantly excited by a given design condition. For illustration, the several

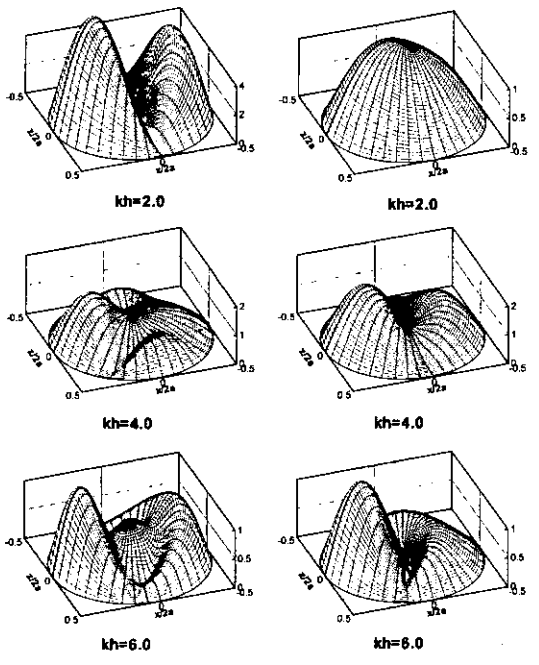

(a) d/h = 0.1 (b) d/h = 0.2

Fig. 16. Comparison of dimensionless membrane responses ($|\xi|/A$) for $T/\rho gh^2$=0.02, a/h=0.5.

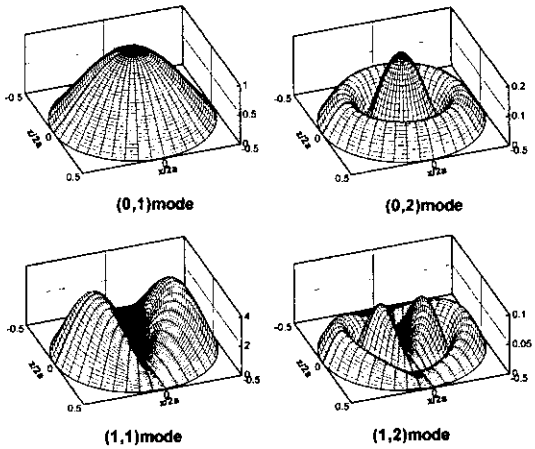

Fig. 17. Comparison of dimensionless modal amplitudes (normalized by incident wave amplitude) for $T/\rho gh^2$=0.02, d/h=0.1 a/h=0.5 at k_1h=2.0.

selected modal amplitudes of the case of Fig. 16(a) are plotted in Fig. 17. It is seen that the (1,1)-mode is dominant over other modes in this case, and therefore the resulting response resembles this mode.

4. CONCLUDING REMARKS

The interaction of incident monochromatic waves with a tensioned, flexible, circular membrane submerged horizontally below the free surface is investigated in the frame of three-dimensional linear hydro-elastic theory. The fluid domain is divided into three regions, and the diffraction and radiation potentials in each region are expressed by the Fourier Bessel series. The displacement of circular membrane is expanded with a set of natural functions, which satisfy the membrane equation of motion and boundary conditions. The unknown coefficients in each region are determined from matching conditions. The numerical result of infinite-tension case is in good agreement with Yu and Chwang's (1993) rigid-disk results.

It is found that the radiated waves generated by membrane motions significantly affect the overall free-surface pattern unless the membrane is deeply submerged or its tension is very large. The tension, radius, and submergence depth of circular membrane are important design parameters in determining phase reinforcement or cancellation between diffracted waves and motion-induced waves. The phase reinforcement results in wave focusing,

as pointed out by Yu and Chwang (1993). The results show that various types of wave focusing are possible for given wave conditions by controlling the size, submergence, and tension of membrane. The free-surface shapes are significantly influenced by dominant membrane modes and the effects increase as membrane flexibility increases and submergence depth decreases. The results also show that the hydrodynamic forces on the flexible disks are generally larger than those on the rigid disks due to the additional loading induced by elastic motions.

REFERENCES

Abramowitz, M. and Stegun I.A.,1972. *Handbook of Mathematical Functions*, Dover, New York.

Cho, I.H., Kee, S.T., and Kim, M.H., 1998. Performance of dual flexible membrane wave barriers in oblique waves, *J. Waterway, Port, Coastal and Ocean Engrg.*, **124**(1), pp. 21-30.

Cho, I.H. and Kim, M.H., 1998. Interactions of a horizontal flexible membrane with oblique waves, *J. Fluid Mech.*, **367**, pp. 139-161.

Chwang, A.T. and Wu, J., 1994. Wave scattering by submerged porous disk, *J. Engrg. Mech.*, **120**, pp. 2575-2587.

Kee, S.T. and Kim, M.H., 1997. Flexible membrane wave barrier. Part 2. Floating/ submerged buoy-membrane system, *J. Waterway, Port, Coastal and Ocean Engrg.*, **123**(2), pp. 82-90.

Kim, M.H. and Kee, S.T., 1996. Flexible membrane wave barrier. Part 1. Analytic and numerical solutions, *J. Waterway, Port, Coastal and Ocean Engrg.*, **122**(1), pp. 46-53.

Lee, J.F. and Chen, C.J., 1990. Wave interaction with hinged flexible breakwater, *J. Hydr. Res.*, **28**, pp. 283-295.

Morse, P.M. and Feshbach, H., 1953. *Methods of Theoretical Physics*, McGraw-Hill.

Thompson, G.O., Sollitt, C.K., McDougal, W.G. and Bender W.R., 1992. Flexible membrane wave barrier, *Proc. Conf. Ocean V*, ASCE, College Station, pp. 129-148.

Williams, A.N., Geiger, P.T. and McDougal, W.G., 1991. Flexible floating breakwater, *J. of Waterway, Port, Coastal and Ocean Engrg.*, **117**(5), pp. 429-450.

Williams, A.N., 1996. Floating membrane breakwater, *J. Offshore Mechanics and Arctic Engrg.*, **118**, pp. 46-51.

Yu, X. and Chwang, A.T., 1993. Analysis of wave scattering by submerged disk. *J. Engrg. Mech.*, **119**, pp. 1804-1817.

Received May 15, 2000
Accepted July 24, 2000